ASIAN JOURNAL OF PHARMACEUTICAL AND CLINICAL RESEARCH

INNOVARE ACADEMIC SCIENCES
Knowledge to Innovation

Vol 11, Issue 3, 2018

Online - 2455-3891
Print - 0974-2441

Research Article

SYNTHESIS AND CHARACTERIZATION OF NOVEL SA-PA-LSA/C-30B/AG NANOCOMPOSITES FOR SWELLING, ANTIBACTERIAL, DRUG DELIVERY, AND ANTICANCER APPLICATIONS

NANJUNDA REDDY BH[1,2], PRADIPTA RANJAN RAUTA[3], VENKATALAKSHIMI V[4]*, SWAMY SREENIVASA[2]

[1]Department of Chemistry, Amrita School of Engineering, Amrita Vishwa Vidyapeetham, Bengaluru, Karnataka, India. [2]Department of Studies and Research in Chemistry, Tumkur University, Tumkur, Karnataka, India. [3]Department of Chemistry, NIT Rourkela, Department of life Sciences, Rourkela, Odisha, India. [4]Department of Chemistry, AMC Engineering College, Bengaluru, Karnataka, India. Email: laxmimurthy@rediffmail.com

Received: 05 October 2017, Revised and Accepted: 15 December 2017

ABSTRACT

Objective: The main objective of this work was to formulate and evaluate Closite-30B/nanoAg filled hydrogel composites which are further intentended to be used for the study of drug delivery,antibacterial, and anticancer activity

Methods: In this study, Cloisite-30B (C-30B) clay dispersed biopolymer sodium alginate (SA)-grafted-poly (acrylamide [AAm]-co-lignosulfonic acid) hydrogel composites were synthesized by free radical *in situ* polymerization reaction technique using SA, AAm, and lignosulfonic acid biopolymers in different proportions in combination. which are subjected to invitro drug delivery and Minimum inhibitory concentration(MIC) method for antibacterial activity study by using *Streptococcus faecalis* (*S.faecalis*) and *Escherichia coli* (*E. coli*)bacteria. The biocompatibility of the prepared gels were determined by standard protocol HaCaT-cells and MCF-7 cell lines further the prepared hydrogel composites were characterized for particle size,encapsulation efficiency,swelling properties,compatibility studies by FTIR etc.

Results: The formulated hydrogels were characterized by X-ray diffraction (XRD) to analyze the particles size and crystallinity. The presence of functional groups and their chemical interaction with the drug, C-30B, and silver nanoparticles (AgNPs) were confirmed by the FTIR spectroscopy. Furthermore, the presence of AgNPs in the matrix was confirmed by ultraviolet/visible spectroscopy. Thermogravimetric analysis was performed to find out the thermal degradation, thermal stability, and the percentage of weight loss at various temperatures. Swelling studies revealed that C-30B and AgNPs induced composites exhibited higher swelling ratio than pure hydrogels. The hydrogels with C-30B/AgNPs displayed excellent antibacterial activity against both Gram-positive and Gram-negative bacteria. Further, these hydrogel composites were loaded with the drug paclitaxel (PT), and drug release study showed that the sustained release of the drug from C-30B/Ag hydrogel matrix compared to rest of other samples. Hydrogel composites were cytocompatible in nature (with HaCaT cells) and the cell viability decreased (with MCF-7cells) with the presence of lignosulfonic acid as well as C-30B and AgNPs in the samples as evaluated through 3-(4,5-dimethylthiazol-2-yl)-2,5-diphenyl tetrazolium bromide to its insoluble formazan assay.

Conclusion: The synthesized hydrogel composites were successfully characterized and eavaluated for sustained release of paclitaxel drug delivery at different pHs and temperatures and it is found that C30B/Ag filled composites exhibits contolled release of drug with higher rate, especially at lower pH (pH2) and higher temperature (37oC) and the same formulations which exhibits better anitbcterial and anticancer activity compared to the virgin samples So the prepared C30B/AgNPs hydrogels composites used in drug dlivery for the effective treatment of cancer and used against bacterias and cancerous cells.

Keywords: Hydrogel composites, Silver nanoparticles, Cloisite-30B clay, Lignosulfonic acid, Antibacterial activity, Drug delivery, Anticancer studies, Sodium alginate, Biopolymer, Acrylamide.

 DOI: http://dx.doi.org/10.22159/ajpcr.2018.v11i3.22939

INTRODUCTION

In this study, Cloisite-30B (C-30B) clay dispersed biopolymer sodium alginate (SA)-grafted-poly (acrylamide [AAm]-co-lignosulfonic acid) hydrogel composites were synthesized by free radical *in situ* polymerization reaction technique using SA, AAm, lignosulfonic acid biopolymers in different proportions in combination. At present, nanotechnology is very crucial in day-to-day life and improved studies attention on nanocomposite hydrogels due to their hydrophilic nature and their possible biocompatibility and uses in the field of biomedical sciences such as implants, drug delivery systems, and tissue engineering [1-4]. Several distinct systems and strategies were evaluated for drug targeted on to cancer cells over the years. Most commoly used systems comprise of polymers, hydrogels, polymer beads, micells, naoparticles, nanoclays and antibodies are the few instances in passive drug targeting, active drug targeting to cancer cells [5].

Nanocomposite hydrogels may be described as three-dimensional polymer networks slightly crosslinked, swollen with water or organic fluids and that can absorb and retain aqueous solutions up to hundreds of times their own weight in the presence of metal nanoparticles (MNP) and nanoclay [6,7]. The formation of MNP-induced materials in combination with nanoclays has clinical and scientific interests in research in recent years because of their extraordinary and flexible characters. Those characteristics are important for silver as ions, nanoparticles, compounds, etc., and a lot of works have been carried out to study their applications in restricting the entry of microbes in packing materials, drug transport, and water purification. As heavy metallic, Ag^0, Ag^+ ions are accountable for inactivation of proteins in microbes through reacting with thiol groups (-SH) of the bacterial membrane results in the death of microbial cells [8-10]. The biological activity, inclusive of the antibacterial activity of Ag^0, relies upon on its size. For that reason, silver nanoparticles (AgNPs) have to be small enough to penetrate into the cell membrane [11]. Ag ions can kill bacteria right away using ultimate their enzymatic breathing structures, without inflicting any harm to human cells. Even though nanocomposites having MNP have well-designed features. Due to high surface free

energy, homogeneous distribution of MNP is difficult, which may root to agglomeration. Therefore, research on such nanocomposites with preferred property is an important issue.

Thus, to prepare such nanocomposites with AgNPs of controlled size could be achieved by reduction of metal ions into MNP in the hydrogels [12-14]. SA is a salt of alginic acid, natural, biodegradable polymer, obtained from seaweeds and consists of 1→4, linked D-mannuronic acids and L-glucuronic acid residues set as blocks of either type of unit or as an arbitrary distribution of each type [15]. Moreover, extensively used as a hydrogel constituent because of its improvements in hydrophilicity, high swellability, nontoxicity, and easy preparation [16,17]. SA is used extensively used in drug delivery applications due to its remarkable physical properties such as, high water retention capacity which enhance the hydrophilic diffuse surface, and low interfacial tension which reduces the transport resistance for the absorption or release of solutes [18-21]. But SA hydrogels having inadequate strength under physiological environment. Inconvenient and not suitable for sensible use and by having restricted strength under physiological environment [22]. For antibacterial activities targeted toward *in vivo*, the mechanical strengths are vital due to the fact they ought to possess sufficient mechanical elasticity and versatility to face up to compression forces from the encircling tissues *in vivo* without any damage. To enhance its mechanical strength, SA is blended with another polymer such as lignosulfonic acid (LSA). LSA is a natural polymer formed from the byproduct of plant resources; however, it is a sulfite cooking of timber and is a waste product from pulp and paper industry.

C-30B, montmorillonite (MMT) is a member of the smectite group minerals (belongs to the class of 2: l phyllosilicate clays) which has a layered silicate platelets. MMT has been significantly implemented for extended release of drugs as it could hold large amounts of the drug due to its excessive cation exchangeability. The surface adsorption of various drugs to MMT clay improves their solubility rate. The hydrophilic and swelling properties of MMT in aqueous media help to ease the wetting of hydrophobic drug substances. This clay eventually improves the bioavailability of drugs [23].

Paclitaxel (PT) is an anticancer drug separated from the bark of the Pacific yew tree, Taxus brevifolia [24]. It has been used in lots of cancers treatments which include breast cancer, ovarian cancers, lung cancer, head and neck carcinomas, and acute leukemia. It binds to the β-subunit of the tubulin heterodimer resulting in the length of the cell partition cycle between the prophase and anaphase degrees, later principal to apoptosis of the most cancers cells [25]. Due to its limited solubility, PT in an adjuvant known as cremophor EL, which leads to graveside effects inclusive of hypersensitivity reactions, nephrotoxicity, neurotoxicity, and cardiotoxicity [26,27]. Lately, type of restrained release pattern was proven to increase its dissolution and reduce the ill effects further to prevent the usage of the poisonous adjuvant [28-31].

In this study, hydrogel composites of SA, LSA, and poly AAm (PA) were successfully synthesized by means of *in situ* polymerization reaction by dispersing C-30B into the solution. The consequent composite hydrogels are used as nanoreactors for the synthesis of AgNPs. This is a totally an innovative method of research for the formation of AgNPs from C30B clay induced SA-PA-LSA blend polymer matrix or network and try to intercalate or exfoliate the polymer chains in to the gallery of clay platelets in order to improve its drug delivery,antibacterial properties as well as anticancer activity and very littele work has been done so far in this particular field as per literature servey. Further, these composites were effectively used in the swelling, antibacterial, anticancer, and drug delivery studies and further characterized by Fourier transform infrared (FTIR), X-ray diffraction (XRD), thermogravimetric analysis (TGA), and ultraviolet (UV) techniques.

EXPERIMENTAL

Materials

Sodium alginate, lignosulfonic acid, Acrylamide(AAm), N,N'-methylenebisacrylamide (MBA) as crosslinking agent, N,N,N',N'-Tetramethylethylenediamine (TEMED) as an accelerator, potassium persulfate (KPS) as an initiator, sodium borohydride ($NaBH_4$), methanol and commercial modified nanoclay (C-30B), and silver nitrate ($AgNO_3$) all the chemicals were procured from Sigma-Aldrich Bangalore, Karnataka, India is used in this experiment as received without any further purification and always double-distilled water (DDW) was used throughout this experiment.

Methods

Dissolve 3 g of SA in 100 ml of DDW stirred for 2 h using the magnetic stirrer to get SA (SA-solution) stock solution. Another stock solution of LSA was prepared by dissolving 600 mg of LSA in 50 ml of DDW separately using magnetic stirrer for 30 min to get LSA-solution, later about 30 ml of SA-solution (0.9 g in 30 ml DDW), LSA-solution, (180 mg of LSA in 20 ml of DDW). In the ratio (SA:LSA) 1:0.5 are mixed together to form SA-LSA solution. Further 5% wt./wt. the ratio of C-30B (45 mg in 10 ml of DDW separately magnetically stirred for 1 h followed by 30 min ultrasonication), dispersed in SA-solution and SA-LSA solution separately [32]. For the resulting solutions, KPS (130 mg in 5 ml DDW), 1 g of AAm in 5 ml of DDW, MBA (130 mg in 5 ml of DDW), and TEMED (130 mg in 5 ml of DDW) are mixed thoroughly and stirred using magnetic stirrer with a gradual increase in temperature, when the temperature reaches about 65–70°C. The entire mixture undergoes *in situ* free radical polymerization reaction to form hydrogels. The obtained hydrogel samples are recovered and cut into desired shapes and left undisturbed in fresh distilled water for 2 days to remove the unreacted chemical constituents, later some of the samples are loaded with AgNPs by allowing them in 0.01N $AgNO_3$ solution for overnight. The $AgNO_3$ is diffused into pores of hydrogels and converted into silver ions and they, in addition, have interaction with polymer chains and clay groups. This is ensured by the conversion of hydrogels from whitish to reddish brown color which confirms the formation of silver ions (Ag^+ ions) in the gel networks, further, these silver ions are converted to AgNPs inside the gel network in the presence of $NaBH_4$ reducing agent. After 30 min, the appearance of dark gray gels indicates the complete reduction of Ag^+ ions into AgNPs (Ag atoms), further, these hydrogels are washed with distilled water and followed by methanol and dried at ambient temperature and used for drug delivery, antibacterial study, and other characterizations.

RESULTS AND DISCUSSION

Swelling studies

Results

The swelling property of C-30B clay supported SA-PA, SA-PA-LSA/C-30B, and SA-PA-LSA/C-30B/AgNPs hydrogel composites as shown in F**ig.** 1 The graph is plotted % of swelling fraction versus various samples such as SA-PA, SA-PA-LSA/C-30B, and SA-PA-LSA/C-30B/Ag composites. The pre-weighed piece of gel samples (0.1 **g**) of each were immersed in a 50 mL of de-ionized water and were equilibrated in distilled water at 25°C for **3** days until equilibrium swelling was achieved. The swelling ratio (Q) of the gels was calculated from the Equation (1) [33].

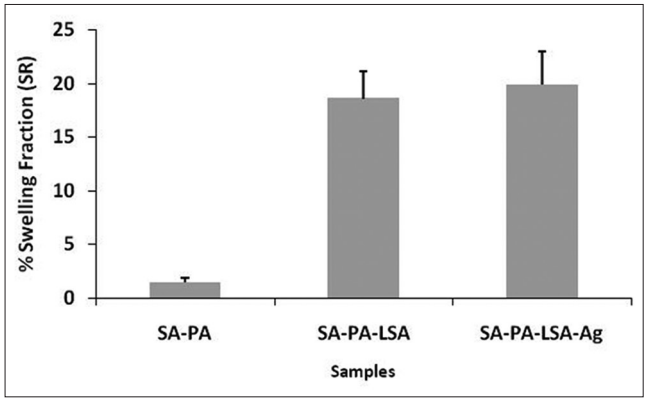

Fig. 1: Effect of swelling behavior of cloisite-30B clay supported sodium alginate (SA)-polyacrylamide (PA), SA-PA-lignosulfonic acid (LSA), and SA-PA-LSA-silver

$$Q = \frac{W_e}{W_d} \quad (1)$$

Where Q is the swelling ratio,
W_e are the weight of water in the swollen hydrogel
and W_d is the dry weight of the hydrogel.

Here we study the water absorbency of hydrogel composites in terms of swelling ratio and swelling percentage. After swelling, the whole gel is gently wiped on both sides using filter paper. The values of W_e, W_d, and Q are calculated.

Discussion

The sample SA-PA (pure hydrogels) indicates least swelling ratio of around less than 3%, this is because absence of both C-30B and AgNPs in them makes much less porous and hence holds less water, whereas SA-PA-LSA with C-30B shows 17–18% of swelling fraction when compared to pure SA-PA hydrogel samples.

This indicates that the presence of hydrophilic clay improves the pore sizes in crosslinked hydrogel networks thereby absorbs and holds more water [34]. Consequently, the sample SA-PA-LSA/C-30B/Ag suggests, the higher swelling ratio compared to rest, again the influence of C-30B and AgNPs together in the SA-PA-LSA/C-30B/Ag hydrogel composites which are responsible for the further increase in the percentage of swelling ratio up to 20%. Which may be due to more porous nature of the resulting hydrogel composites caused by the presence of C-30B/AgNPs.

Antibacterial activity

The antibacterial activities for all the samples SA-PA, SA-PA-LSA/C-30B, and SA-PA-LSA/C-30B/AgNPs, have been studied for *Streptococcus faecalis* and *Escherichia coli* were shown in Fig. 2.

Results

The minimum inhibitory concentration (MIC) was determined by the following CLSI procedure for the broth microdilution method [35]. The bacterial lines have been cultured onto Luria Bertani Agar medium (containing 0.5% peptone, 0.5% yeast extract, 1% NaCl and 1.5% Agar, at pH 7.5±0.2). The reserve solution was obtained by allowing the 10 mg of gel in 10 ml phosphate buffered saline (PBS) (phosphate buffer 67 mM, pH 7.4, 0.05% Tween 20, and 0.02% sodium azide) filled in small vials. The gel particle solutions have been incubated at 37°C underneath mixing for 24 h [36]. Supernatant samples of 500 µl have been accrued by centrifugation and saved at 4°C before screening for antimicrobial activities. Chloramphenicol, an antibiotic, was used as the best manipulate and PBS was used, because of the –ve charge. The resulting cultures were added to the sterilized Mueller-Hinton Broth (MHB) (containing 30% red meat extort 1.75% casein acid hydrolysate and 0.15% starch, pH 7.4±0.2).

The MIC was determined by means of the use of serial twice diluted in the medium (MHB) having 1.95–1000 µg/ml of the trial samples. To every well of 96 well microtiter plate, 150 µl of medium (MHB) was used as the spare sample, to which 10 µl of 0.5 McFarland (1.5×108 CFU/ml) cultured microorganisms from MHB has been introduced. The inoculated plates had been incubated at 37°C for 24 h. After incubation, the bacterial growth was monitored by measuring the turbidity of the culture using microtiter plate optical colorimeter (OD600). The MIC became determined as the lowest concentration of compound at which the visible growth of the organisms becomes completely inhibited. The results of experimental assays were expressed as mean value ± standard error. Student test or one-way analysis of variance followed by Duncan's multiple range tests was performed using SPSS18 software to compare the variations in various parameters at a significance level of difference ($p<0.05$).

Discussion

In Fig. 2 it is found that sample SA-PA-LSA/C-30B/AgNPs indicating higher antibacterial activity ($p<0.05$) against both the bacteria *S. faecalis* and *E. coli* (MIC is 1.14±0.74 µg/mL) compared to *S. faecalis* (MIC is 3.25±1.13 µg/mL) because AgNPs are the most used antimicrobial particles in polymeric nanocomposites [37] as shown in Table 1.
This is due to the release of ions from the surface of nanoparticles and bacteria dies as the ions bind to the cell membrane. The Ag+ ions released from the surface of the nanoparticles may interact with the thiol groups present in the proteins leads to loss of their replicability, inactivation of bacteria and condensation of DNA molecules [38].

Nano Ag appears to be significantly more efficient in mediating their antimicrobial activities [39]. It is observed from the data presented in Table 1, the antibacterial activity of SA-PA-LSA/C-30B is comparatively less compared to SA-PA-LSA/C-30B/Ag because the presence of C-30B/Ag with LSA causes more activity, while in the case of the pure sample which shows the least activity against both the bacteria because of the absence of AgNPs as well as C-30B/LSA in the sample. The antibacterial activity follows the following order with respect to various samples are SA PA-LSA/C-30B/Ag >SA-PA-LSA/C-30B>SA-PA.

UV/visible (UV-Vis) spectroscopy

The UV-vis absorption spectra for the formation of SA-PA, SA-PA-LSA/C-30B, and SA-PA-LSA/C-30B/Ag composite as proven in Fig. 3a-c. In Fig. 3c, the intensity of surface plasmon resonance absorption peak corresponding to AgNPs was steadily expanded with a mild shift in the wavelength of the peak 410–420 nm [40]. This absorption peak indicates the formation of AgNPs of smaller length with narrow size distribution [41]. Whereas no such peaks are observed for other two samples SA-PA and SA-PA-LSA/C-30B which indicates the absence of Ag nanoparticles in them. The SA-PA-LSA impacts the reduction as

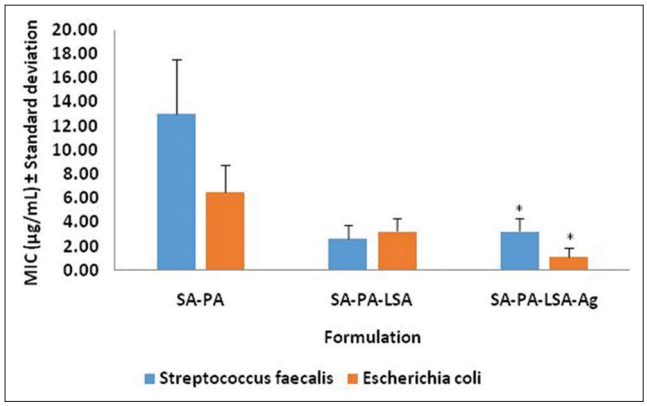

Fig. 2: Antibacterial activity of sodium alginate polyacrylamide (SA-PA), SA-PA-lignosulfonic acid (LSA)/C-30B, SA-PA-LSA/cloisite-30B (C-30B)/silver *Escherichia coli*, and *Streptococcus faecalis*. Data are expressed as the mean±standard deviation (n=3) *p<0.05

Table 1. Antibacterial activity data of SA-PA, SA-PA-LSA/C-30B, SA-PA-LSA/C-30B/Ag

Sl. No	Formulations	MIC (µg/mL)±Standard deviation	
		S. faecalis	*E. coli*
1	SA-PA	13.02±4.51	6.51±2.26
2	SA-PA-LSA/C-30B	2.60±1.13	3.25±1.13
3	SA-PA-LSA/C-30B/Ag	3.25±1.13*	1.14±0.74*

Data are expressed as the mean±standard deviation (n=3). *p<0.05.
SA: Sodium alginate, PA: Polyacrylamide, LSA: Lignosulfonic acid,
C-30B: Cloisite-30B, MIC: Minimum inhibitory concentration, *E. coli: Escherichia coli, S. faecalis: Streptococcus faecalis*

well, because of the stabilization of AgNPs in the presence of inorganic reducing agent NaBH4.

In Fig. 3c, it is observed that formation of Ag nanoparticles in the network of SA-PA-LSA hydrogel is readily reduced by $NaBH_4$ and immediately turn into brown color. It indicates that the Ag nanoparticles were formed and entrapped inside the polymeric SA-PA-LSA hydrogel networks.

FTIR spectroscopy studies

FTIR spectra of SA-PA, SA-PA-LSA/C-30B, and SA-PA-LSA/C-30B/Ag hydrogels were shown in Fig. 4a-c. The band at about 3736.6/cm is due to the -OH stretching vibrations indicating the presence of H-bonding between SA-PA-LSA polymers causing OH/NH_2 stretching [42]. The band at 1653.7/cm is assigned to carbonyl stretching conjugated with the aromatic ring. At the 1637/cm H-O-H bending, typically, H- bond occurred between proton donor and proton acceptor atoms. The lone pair of electrons -O- of PA may seek interaction with -H atoms of SA and formed intermolecular asymmetrical stretching vibrations at 1653.77/cm in SA showed the presence of –COO group. The characteristic band at 1647/cm was due to amide group (–CONH2) of PA (>C=O stretching) [43]. The intermolecular hydrogen bond provides an additional mechanical strength to the grafted polymer; these differences supported the successful grafting of AAm in SA. Absorption at 1438.7/cm indicates the C-H deformations. The bands at 1103.4/cm and 955.16/cm are the representative vibrations of the sulfonic group. The absorption peaks at 1308.6/cm imply C-O stretch and the existence of the peak at 1308/cm due to the complexation between the amino groups of the SA-PA and SA-PA-LSA/C-30B/Ag composites. The band at 1202/cm represented the C–N stretching vibration of hydrogel units. The absorption band at 1036.4/cm is due to the vibrational stretching of the -SO3H group of SA-PA-LSA unit [44,45].

The absorption peaks at 2927.0/cm indicate C-H stretch. The Ag nanoparticles loaded SA-PA-LSA hydrogels Fig. 4 have proven all the above functional peaks with a slight shift of the height 132–1352/cm corresponding to amide III bands. In addition, the stretching vibration at 3180.5/cm similar to OH/NH2 groups, has shifted to 3423/cm, indicating that the silver particles are bonded to the functional groups present each in SA, PA, and LSA polymer chains. However, in the case of AgNPs loaded hydrogels and SAPA there may be a slight change in the vibrational frequencies (Fig. 4a and c). The characteristic features of the spectrum of Ag nano hydrogel composites are all most very similar to those of plain polymer [46].

XRD analysis

XRD characterization of the structure of nanocomposites is evaluated by means of XRD dimension. XRD patterns were considering a Bruker AXS D8 Advance Diffractometer with Cu, radiation at a wavelength of λ=1.5406 A°, at 40 kV and 30 mA. Configuration vertical 2θ, Angle range 360°, usable angular range 3°–135° and detector used Si (Li) PSD. SA-PA-LSA/C-30B/Ag hydrogel composites were scanned over the range of diffraction angle 2θ=1–80°, with a scan speed of 1°/min at room temperature. Powder samples were pressed into a tablet-shaped disc before XRD analysis.

Results

The XRD spectroscopy patterns form of SA-PA, SA-PA-LSA, and SA-PA-LSA/Ag hydrogel composites which are obtained from *in situ* free radical polymerization synthesis technique are as shown in Fig. 5a-c. The XRD patterns were composed of 5°–80° (2θ). It can be seen that C-30B shows some characteristic peaks at 2θ=9.09° (0.97 nm), 19.83° (0.45 nm), 28° (0.32 nm), 35° (0.26 nm), 43° (0.21 nm), and 62° (0.15 nm), respectively.

Discussion

The XRD spectrum of pure C-30B indicates a strong peak at 2θ=9° which corresponds to a basal spacing of 0.98 nm [47]. After the reaction, this peak has almost disappeared, and other diffraction peaks are similar to those of pure C-30B, and 2θ remains unchanged. In other words, we detected no peak for the composites prepared from C-30B, which implies that they all possess exfoliated structures in the composite. Similar results are obtained in some reported papers [48,49]. Results obtained indicate that MMT has been finely dispersed in the polymer matrix, and the copolymerization reaction is performed on the surface of C-30B. These results are consistent with the results obtained from scanning electron microscopy.

Further the peaks appear at 2θ values of 27.41, 31.72, 37.71, 43.94, 45.86, 57.12, 62.76, and 77.0 corresponded to the planes (111), (200), (220), (222), and (311) of SA-PA, SA-PA-LSA/C-30B and SA-PA-LSA/C-30B/Ag composite [50]. The diffraction peaks at 2θ of 37.7° and 43.94°, which can be ascribed to the (111) and (200) crystallographic planes of face-centered cubic silver crystals, respectively [51].

The average particles sizes of SA-PA, SA-PA-LSA/C-30B, and SA-PA-LSA/C-30B/Ag hydrogel composites were sited to be 19.8, 19.0, and 14.2 nm that is calculated using Debye Scherrer equation [52] as shown in Table 2.

TGA

The thermal stability of hydrogels composites of SA-PA, SA-PA-LSA/C-30B hydrogel, and SA-PA-LSA/C-30B/Ag have been investigated by way

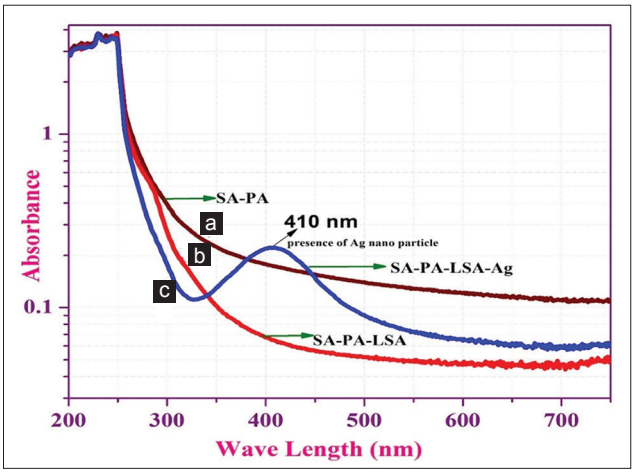

Fig. 3: Ultraviolet-visible spectra for (a) sodium alginate (SA)-polyacrylamide (PA), (b) SA-PA-lignosulfonic acid (LSA) (c) SA-PA-LSA-silver

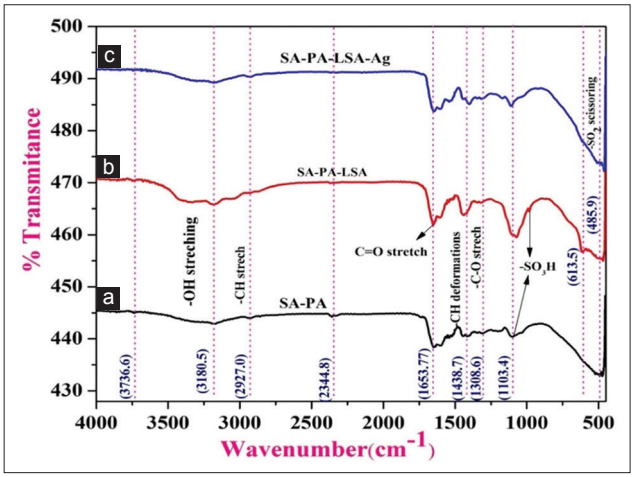

Fig. 4: Fourier-transform infrared spectra of (a) sodium alginate (SA)-polyacrylamide (PA) (b) SA-PA-lignosulfonic acid (LSA)/ cloisite-30B (C-30B) (c) SA-PA-LSA/C-30B/silver

of TGA as shown in Fig. 6a-c. In Fig. 6, the first stage of decomposition is attributed to the weight reduction of residual moisture, and the initial decomposition of the hydrogel chains took place around 230°C. About 80% weights the reduction took place at 420–430°C for both the hydrogel composites, besides SA-PA hydrogel. A clear distinction has been determined in TGA experiments, in that SA-PA-LSA/C-30B/Ag hydrogel composites shows better thermal stability than the pristine hydrogel. The difference in thermal decomposition of the pure hydrogel and the C-30B/silver nanocomposite hydrogels are found to be ~15%, which shows that the formation of AgNPs within the hydrogel network. A large number of AgNPs modified into shape inside the hydrogel. It has been found from the graphs, SA-PA exhibits least thermal stability as this sample is free from both C-30B and AgNPs. Some reported works [53,54] give another reason for the higher thermal stability of the nanocomposite hydrogel in comparison with the clay-free hydrogel composites, namely, that thermal stability is attributed to crosslinking formation between the clay and growing chains of the polymer and shows 60% weight reduction at 400°C due to thermal decomposition of polymer chains of both SA, LSA, and PA with the evaporation of embedded water molecules [55]. Further, it is observed that there are four levels of (multistage) degradation; the first stage is likely due to moisture present in the sample that is absorbed from an external environment, across the temperature of a 180°C. The second stage of thermal degradation starts at 200°C and end up with the temperature of 250°C. This may be due to the decomposition of crosslinks between the SA, LSA, and PA [56,57]. The next stage (third stage) of decomposition begins at 250°C and ends up with 330°C and, finally, the last major stage which (fourth stage) starts at 330°C and stops at 400°C ascribed to complete decomposition of polymer chains and confirms the formation of ash with carbon content indicated by constant and linearity remains same for the graph line. 50% of weight loss was observed when the temperature increases up to 800°C (range of temperature is 400–800°C). Hence, a similar type of thermal decomposition pattern is observed in other two samples such as SA-PA-LSA/C-30B and SA-PA-LSA/C-30B/Ag [58].

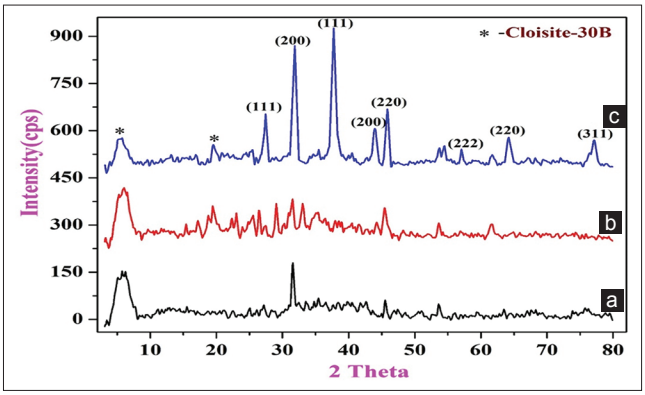

Fig. 5: XRD spectra of (a) sodium alginate (SA)-polyacrylamide (PA) (b) SA-PA-lignosulfonic acid (LSA)/cloisite-30B (C-30B) (c) SA-PA-LSA/C-30B/silver

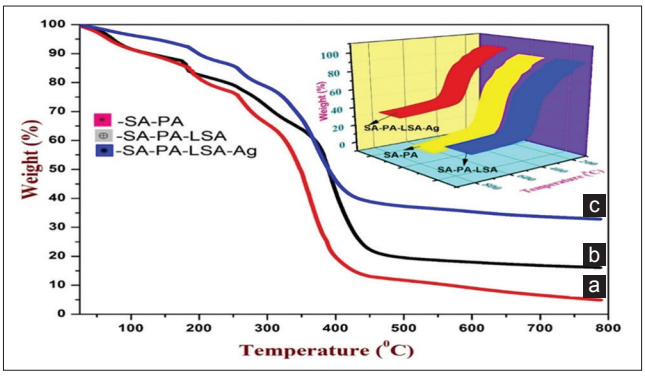

Fig. 6: Thermogravimetric analysis curves of (a) sodium alginate (SA)-polyacrylamide (PA) (b) SA-PA-lignosulfonic acid (LSA)/ cloisite-30B (C-30B) (c) SA-PA-LSA/C-30B/silver

Table 2: Average crystallite size of SA-PA, SA-PA-LSA/C-30B, and SA-PA-LSA/C-30B/Ag

Sample	FWHM (rad)	Average crystallite size (nm)
SA-PA	0.42	19.88
SA-PA-LSA/C-30B	0.4	19.0
SA-PA-LSA/C-30B/Ag	0.59	14.2

SA: Sodium alginate, PA: Polyacrylamide, LSA: Lignosulfonic acid, C-30B: Cloisite-30B, Ag: Silver

Drug delivery study

Encapsulation efficiency

The dried samples of hydrogel composites are kept in PT drug solution overnight so that the composites swell within the drug solution and resulting swollen hydrogel composites dried at an ambient temperature, further which is used *in vitro* drug release study. PT encapsulation efficiency is calculated, and PT encapsulation efficiency depends on the polymer type and the physical state of the drug for the duration of processing. The loading efficiencies have been decreased with the presence of clay as well as AgNPs as shown in Table 3.

In case of SAPA, the drug encapsulation efficiency became 72.4±3.17% which is significantly higher in comparison to SA-PA-LSA/C-30B/Ag ($p<0.05$). The higher % of encapsulation efficiency may be due to the absence of crosslinking density which is caused by the presence of C-30B [32,59]. The most of the pores are occupied by AgNPs and cross-linking of C-30B with polymer chains results in absorption of less amount of drug and decreases the encapsulation efficiency in the case of SA-PA-LSA/C-30B and SA-PA-LSA/C-30B/Ag hydrogel composites. Hence, this may be due to the fact that the presence of LSA, C-30B, and AgNPs in SA-PA influences on encapsulation efficiency and hence more amount of drug is absorbed by SA-PA hydrogel composite. Hence, the encapsulation efficiency was decreased to 62.5±6% in the case of SA-PA-LSA/C-30B. Further after the formation of AgNPs in the hydrogel composite network whereas, the encapsulation efficiency is further reduced to least value 56.5±4.

In vitro drug release study: Effect of pH, temperature, and time on drug release

Results

The effect of pH on PT drug release at pH 2 and pH 7.2 with temperature 25°C and 37°C for SA-PA, SA-PA-LSA/C-30B, and SA-PA-LSA/C-30B/Ag hydrogel composites were shown in Fig. 7a-d. Indicates that there is an increase in PT release profile at various timings (duration of PT release) for all formulations at pH 2 (gastric media) and 7.2 (intestinal fluid) at the temperature 37°C. The initial burst release of PT was observed within 4 h which is about 28%. This indicates that some part of PT is primarily associated with nanocomposites remain on their surfaces by weak interaction forces between SA-PA-LSA/C-30B/Ag composite hydrogels and PT.

Table 3: Percentage of encapsulation efficiency of SA-PA, SA-PA-LSA/C-30B, and SA-PA-LSA/C-30B/Ag

Sl. No.	Code	Encapsulation efficiency (%)
1	SA-PA	72.4±3.17
2	SA-PA-LSA/C-30B	62.5±6
3	SA-PA-LSA/C-30B/Ag	56.5±4*

Data were expressed as mean value±standard deviation (n=3).*$p<0.05$.
SA: Sodium alginate, PA: Polyacrylamide, LSA: Lignosulfonic acid, C-30B: Cloisite-30B, Ag: Silver

Cumulative release reports show increasing the pH from 2 to 7.2, the considerable decrease in the cumulative release of the drug is observed from all the formulations. The release of drug PT after 8 h from all formulations at pH 2 is ~36.17% while drug delivery after 12 h is ~47.06%, drug release after 24 h is ~60.3%, drug delivery after 42 h is ~67.41%, and drug delivery within 72 h is ~ 81.3% at pH 2, and it is found from the graphs linearity has been established from 42 h to 72 h which suggests that drug release remains regular and constant during at that period at pH 2 (% of drug release after 8, 12, 24, 42, and 72 h is in the order ~36.17%, ~47.06%, ~60.3%, ~67.41%, and ~ 81.3%, respectively, at pH 2).

The discharge of drug PT after 8 h from all formulations at pH 7.2 is ~35.3%, drug release after 12 h is ~44.62%, drug release after 24 h is ~54.65 %, drug release after 42 h is ~64.7%, and drug release within 72 h is ~76.39%, and it is found from the graphs linearity has been achieved from 42 h to 72 h which indicates that the drug release remains constant and steady during that range of time and at pH7.2 (% of drug release after 8, 12, 24, 42, and 72 h, is in the order ~35.3%, ~44.62% ~54.65%, ~64.7%, and ~76.39%, respectively).

Discussion

Effect of pH

The increasing order of drug release at pH 2 and pH 7.2 is in the following order, SA-PA-LSA/C-30B/Ag>SA-PA-LSA/C-30B> SA-PA. In contrast to SA-PA, because of the absence of both C-30B and AgNPs in SA-PA which makes the hydrogel composite less porous and decrease in crosslinking density which is responsible for less swelling of SA-PA hydrogel composite in the buffer media and hence less amount of PT is released from SA-PA with slower rate compared to other formulations. And also it was hypothesized that incorporation of drug moiety within these polymeric carriers is able to deliver the drug in a sustained manner [60]. Further the higher rate of PT release at pH 2 compared to pH 7.2 may be due to the presence of AgNPs and the negative charges on the clay (C-30B) decreases with the decrease in pH, it has also been well reported that more chain relaxation took place in the basic environment compared with acidic conditions [61,62]. Which indicates that drug, binds firmly to clay/AgNPs and loosely to SA-PA polymer amide chains and therefore it is released slightly faster and more quantity from SA-PA-LSA/C-30B and SA-PA-LSA/C-30B/Ag at pH 2. The presence of C-30B and AgNPs in SA-PA hydrogel matrix influenced the interaction of drug PT with SA-PA and accelerated the release of drug from SA-PA-LSA/C-30B and SA-PA-LSA/C-30B/Ag hydrogel composites.

Thus, drug release was comparatively faster from the hydrogel composite than pure SA-PA hydrogels at both the pHs. And also the nanocomposite hydrogel containing silver (AgNPs) showed profound PT release in acidic (pH 2) medium than intestinal medium (pH 7.2). This suggests that the drug release within the pure SA-PA hydrogel and SA-PA hydrogel composites can be virtually used in the acidic gastric environment.

Effect of temperature

Temperature has some effect on the drug release property of the SA-PA-LSA/C-30B/Ag composite hydrogels. At 25°C, the hydrogel composites are, however, in a swollen condition, and the PT release especially is based on at the diffusion, and the drug delivery from all formulations is pretty slow. At 37°C, PT delivery from the all the formulations is quicker than at 25°C. The prolonged drug release at 37°C is attributed to the collapse of the hydrogel shell. Moreover, the loaded PT drug became squeezed (together with water) and comes out of the composite hydrogels. And consequently, these composites are pH sensitive and temperature sensitive which proficiently promises the anticancer PT drug delivery.

Fig. 7 % cumulative release of paclitaxel through sodium alginate (SA)-polyacrylamide (PA), SA-PA-lignosulfonic acid (LSA), SA-PA-LSA-silver (Ag)

(a) at pH=2, temperature 37°C, (b) at pH=2, room temperature 25°C (

c) at pH=7.2, temperature 25°C, (d) at pH=7.2, room temperature 25°C

The effect of time

For all formulations as time increases the release profile of PT also increases exponentially from 4 to 72 h at all pH and temperatures. All formulations show an initial burst release of PT within 4 h ~28% whereas ~36.4% of PT is released from all formulations within 8 h, after 12 h 48.84% of PT release was observed, drug release after 24 h, is 57.47%, while drug release after 42 h, is 66.52% and drug release within 72 h, is 78.83%. Hence, the time has some influence on PT release, ie., as the time increases the release rate of PT also increases exponentially until a particular time.

About 27% PT is released from all hydrogel composites at pH 7.2 within four h, whereas much <30% of the drug is delivered at pH 2 within 4 h. It looks as if the discharge profile suggests the preliminary burst release which shows that a sizeable amount of PT in the bigining which is associated with nanocomposites remained on their surfaces with the aid of weak interaction forces between SA-PA-LSA/C-30B/Ag hydrogel composites and PT. the discharge half of time T50 at temperature 37°C (time required for releasing 50 wt% of drug) for the SA-PA, SA-PA-LSA/C-30B, and SA-PA-LSA/C-30B/Ag hydrogel composites are 14.32 h, 12.34 h, and 12 h, respectively, at pH 7.2 and the SA-PA, SA-PA-LSA/C-30B, and SA-PA-LSA/C-30B/Ag hydrogel composites are 12.55 h, 12.46 h, and 12.13 h, respectively, at pH 2 and at 37°C. In addition the discharge half of time T50 at temperature 25°C for the SA-PA, SA-PA-LSA/C-30B, and SA-PA-LSA/C-30B/Ag hydrogel composites are 24.86 h, 13.7 h, and 13.73 h, respectively, at pH 7.2 and the SA-PA, SA-PA-LSA/C-30B, and SA-PA-LSA/C-30B/Ag hydrogel composites are 13.59 h,13.1 h, and 12.1 h, respectively, at pH 2.

Drug release kinetics

The drug delivery kinetics of SA-PA, SA-PA-LSA/C-30B, and SA-PA-LSA/C-30B/Ag hydrogel composites had been proven in Tables 4 and 5. The *in vitro* drug discharge had been shown in Tables 4 and 5. The *in vitro* drug discharge have been measured the use of various kinetic models which include zero-order (Equation 1) acquired through measuring the cumulative amount of drug release versus time, first-order (Equation 2) obtained by means of measuring log cumulative percent of drug release versus time, and Higuchi's model (Equation 3) obtained through measuring the cumulative percentage of drug release versus square root of time.

$$C=K_0t \quad (1)$$

Where K_0 is the zero-order rate constant expressed in units of concentration/time and t is the time in hours.

A graph of concentration versus time would produce a straight line with a slope equal to K_0 and intercept the origin of the axes [32,63].

$$\log C = \log C_0 - \frac{Kt}{2.303} \quad (2)$$

Where C_0 is the initial concentration of the drug, k is the first-order constant, and t is the time.

$$Q = Kt\frac{1}{2} \quad (3)$$

Where in K is the constant, indicates the steady reflecting design variables of the system and t is the time in hours.

For this reason, drug delivery rate is proportional to the reciprocal of the square root of time [64].

Mechanism of drug release (data analysis)

The drug release of SA-PA, SA-PA-LSA/C-30B, and SA-PA-LSA/C-30B/Ag hydrogel composites was plotted (Equation 4) as log cumulative percent of drug release versus log time, and the exponent n was calculated through the slope of the straight line [65].

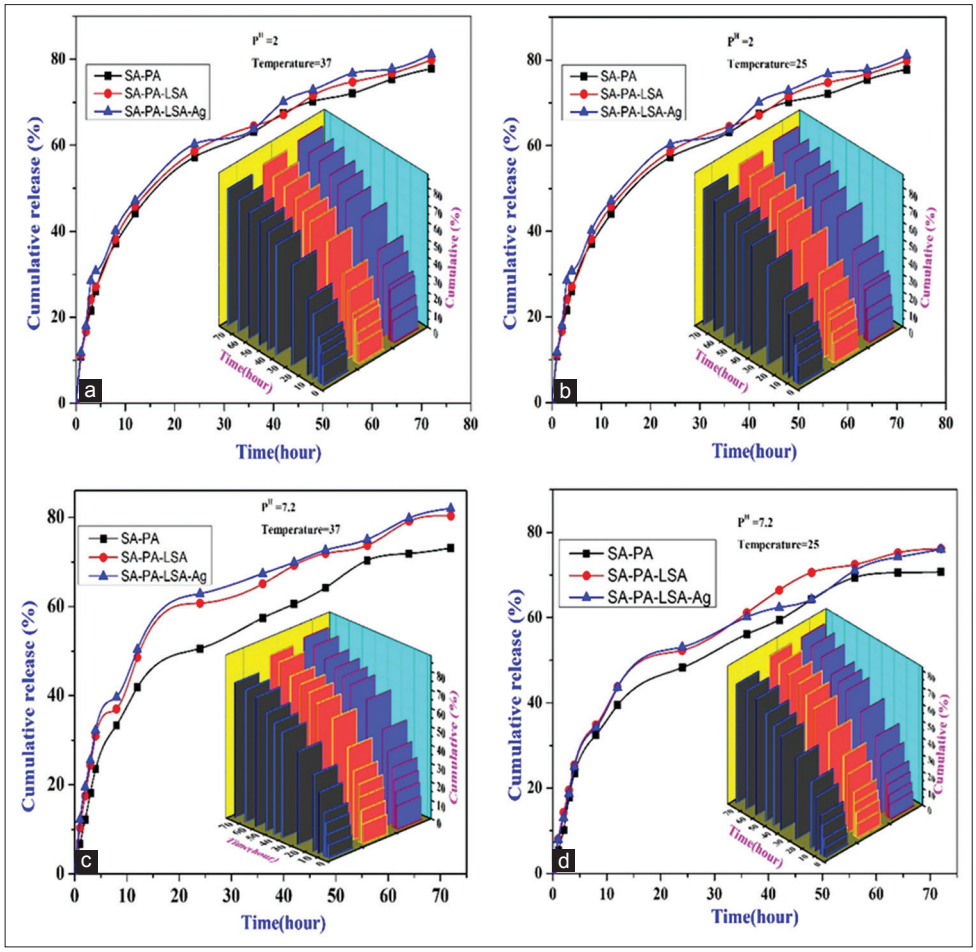

Fig. 7 % cumulative release of paclitaxel through sodium alginate (SA)-polyacrylamide (PA), SA-PA-lignosulfonic acid (LSA), SA-PA-LSA-silver (Ag) (a) at pH=2, temperature 37°C, (b) at pH=2, room temperature 25°C (c) at pH=7.2, temperature 25°C, (d) at pH=7.2, room temperature 25°C

Table 4: Fitting *in vitro* drug release data of different samples according to various mathematical models

Sample	EE %	pH=7.2									
		Zero-order		First order		Higuchi		Hixon Crowell		Korsmeyer–Peppas	
		R^2	K_0	R^2	K_1	R^2	K_H	R^2	k_{hc}	R^2	n
SA-PA	72.3	0.893	0.815	0.966	0.0165	0.976	8.324	0.946	0.02	0.963	0.457
SA-PA-LSA/C-30B	62.5	0.832	0.974	0.949	0.0211	0.962	9.320	0917	0.024	0.956	0.436
SA-PA-LSA/C-30B -Ag	56.5	0.821	0.969	0.947	0.0216	0.957	9.303	0.912	0.025	0.963	0.410

Drug release exponents (n), Korsmeyer–Peppas release constant (K_{KP}), correlation coefficient (R^2), zero-order release rate constants (K0), first-order release constant (K_F) of different models. SA: Sodium alginate, PA: Polyacrylamide, LSA: Lignosulfonic acid, C-30B: Cloisite-30B, Ag: Silver

Table 5: Fitting *in vitro* drug release data of different samples according to various mathematical models

Sample	EE %	pH=2									
		Zero-order		First order		Higuchi		Hixon Crowell		Korsmeyer-Peppas	
		R^2	K_0	R^2	K_1	R^2	K_H	R^2	k_{hc}	R^2	n
SA-PA	72.3	0.834	0.965	0.964	21.25	0.605	0.141	0.918	0.024	0.768	0.727
SA-PA-LSA/C-30B	62.5	0.866	0.904	0.964	0.247	0.831	9.322	0.942	0.024	0.963	0.412
SA-PA-LSA/C-30B-Ag	56.5	0.880	1.00	0.973	0.021	0.975	0.453	0.950	0.025	0.984	0.517

SA: Sodium alginate, PA: Polyacrylamide, LSA: Lignosulfonic acid, C-30B: Cloisite-30B, Ag: Silver

$$\frac{M_t}{M_\infty} = kt^n \quad (4)$$

Where M_t/M_∞ is the fractional solute release,
t is the discharge time,
K is a kinetic constant characteristic of the drug/polymer system, and n is an empirical value, symbolize the discharge method.

Using least square method, we have calculated the values of n and K for all of the three formulations and that information which is shown

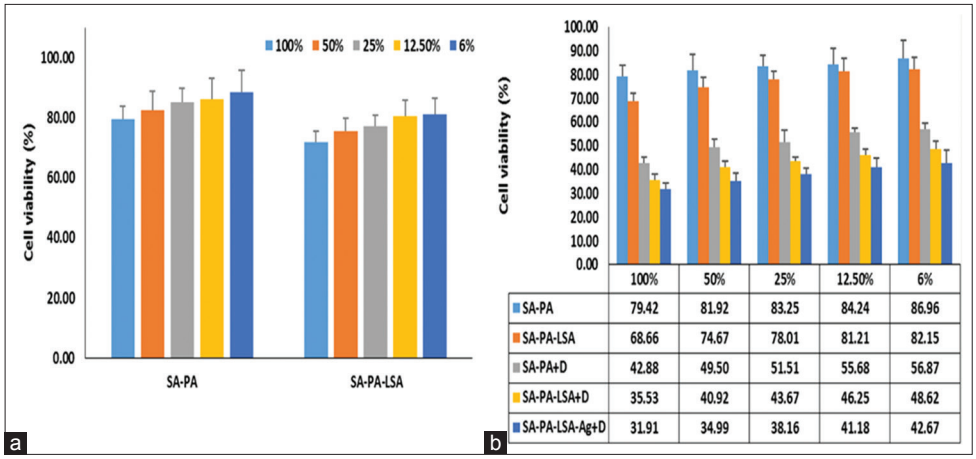

	100%	50%	25%	12.50%	6%
SA-PA	79.42	81.92	83.25	84.24	86.96
SA-PA-LSA	68.66	74.67	78.01	81.21	82.15
SA-PA+D	42.88	49.50	51.51	55.68	56.87
SA-PA-LSA+D	35.53	40.92	43.67	46.25	48.62
SA-PA-LSA-Ag+D	31.91	34.99	38.16	41.18	42.67

Fig. 8: (a) Cell viability of sodium alginate (SA)-polyacrylamide (PA), SA-PA-lignosulfonic acid (LSA) and media at 100% were used as a control. (b) SA-PA, SA-PA-LSA, SA-PA+D, SA-PA-LSA+D, SA-PA-LSA-silver (Ag)+D. Data were expressed as mean value±standard deviation

in Tables 4 and 5. The values of K and n have proven a reliance on the encapsulation performance and nature of the polymer matrix. Values of "k" for composites prepared by means of with and without C-30B, AgNPs ranged from 0.024 to 0.025 in pH 2 and 0.020 to 0.025 in pH 7.2, respectively. However, the drug-loaded composites exhibited "n" values ranging from 0.412 to 0.727 in pH 2 (Table 4) and 0.410 to 0.457 in pH 7.2 (Table 5).

The above values of n and k are indicating swift from Quasi-fickian diffusion type mechanism to non-fickian diffusion (Anamouls) type of mechanism [66]. And the best linearity has been achieved in all models except zero-order kinetic model and samples of SA-PA at pH 2 in Korsmeyer–Peppas method (R^2 = 0.956–0.984) and the diffusion exponent "n" was between 0.412–0.727at pH2 and 0.41–0.457 which seems to indicate the diffusion mechanism is non-fickian diffusion. And suggests that the drug release turned into controlled through more than one system (each diffusion and dissolution) [67].

However, further SA-PA, SA-PA-LSA/C-30B, and SA-PA-LSA/C-30B/Ag hydrogel composites samples follow Higuchi model, which indicates that the drug release is controlled by diffusion of drug through the pores. The mean diffusion exponent value (n) was found to be ranged from 0.410 to 0.457 at pH 7.2 and 0.412 to 0.727 at pH 2 [68]. It is worth to say that the discharge mechanism of a drug would depend on the dosage form, pH, nature of the drug, fillers, and polymer used.

Cytocompatibility assessment by MTT assay

Results

The effect of test nanocomposite hydrogel materials on the cellular proliferation and viability was determined using MTT assay method [69]. The biocompatibility of the prepared gels was determined by the following standard protocol with slight modifications [65]. Briefly, HaCaT and MCF-7 (breast cancer cell lines) cells were procured from NCCS, Pune, India, and the cells were grown in DMEM medium. After 80% confluency, the cells were trypsinized, and 3000 cells/well were seeded in 96 well plates and kept in a CO_2 incubator at 37°C. In the meantime, the prepared hydrogels were cut into small pieces (1 cm×1 cm) and kept inside a dialysis bag, and both the ends were sealed. The dialysis bag was immersed in 20 ml of PBS and was kept in constant stirring at 100 rpm for 24 h. The leachats were from the hydrated hydrogels and were diluted serially with the DMEM media (0%, 12.5%, 25%, 50%, and 100%), and then 200 mL of extracting and the diluted solution was added in a 96-well plate. For the control, 100% media were used to compare among the dilution. The addition of leachats the 96 well plates were subsequently kept in a CO_2 incubator at 37°C. To detect the cell viability, MTT working solution was prepared from a stock solution of 5 mg/mL in growth medium without FBS to the final concentration of 0.8 mg/mL. 100 µL of MTT solution was added and incubated for 4 h. After 4 h of incubation, the MTT solution was discarded, and 100 µL of DMSO solvent was added in each well under dark followed by an incubation of 15 min and the optical density of the formazan product was read at 595 nm in a microplate reader (PerkinElmer, Waltham, MS, USA).

Discussion

In this examine, the cytocompatibility of the organized hydrogels has been tested in normal epithelial HaCaT mobile strains. Fig. 8 suggests the relative proliferation charge of the two cellular lines at the same time as assessed through MTT assay. NAD (P) H-based mobile oxidoreductase enzyme in the mitochondria has the capability to reduce the MTT dye (3-(4, 5-dimethylthiazol-2-yl)-2, 5-diphenyltetrazolium bromide) to insoluble formazan [70].

Fig. 8: (a) Cell viability of sodium alginate (SA)-polyacrylamide (PA), SA-PA-lignosulfonic acid (LSA) and media at 100% were used as a control. (b) SA-PA, SA-PA-LSA, SA-PA+D, SA-PA-LSA+D, SA-PA-LSA-silver (Ag)+D. Data were expressed as mean value±standard deviation

The formation of formazan is predicated on the rate of cellular metabolism, so the cells handled with the specific leachant % need to theoretically have a normal fee of metabolism. These precise gels were cytocompatible in nature. No visible difference turned into observed in the cell morphology, suggesting the absence of the detrimental impact of the leachants on mobile proliferation. Instead, the organized formulations supported the growth of HaCaT cellular line to a certain stage in assessment to the control. Again, cell viability decreases with the presence of LSA/C-30B as well as in the presence of Ag^0 in the hydrogel composites (in MCF-7 cell lines). In Fig. 8a, the MTT assay was used to measure the viability of HaCaT cells at various dilute extract solution concentrations Fig. 8b, the MTT assay was used to measure the viability of MCF-7 cells at various dilute extract solution concentrations.

CONCLUSION

The average particle size of AgNPs in synthesized SA-PA-LSA/C-30B/Ag hydrogel composites was found to be 19.8, 19.0, and 14.2 nm and SA-PA-LSA/C-30B/Ag indicated the highest swelling ratio compared to other samples. The SA-PA-LSA/C-30B/Ag composites show more antibacterial activity against both the bacteria *S. faecalis* and *E. coli* as well as for anticancer activity. From UV absorption spectroscopy wavelength around 410–420 nm confirmed the presence of AgNPs in composites. TGA analysis indicates the decomposition commences at 250°C and ends at 330°C showed that complete decomposition of polymer chains. The presence of LSA, C-30B, and AgNPs indicate absorption of less amount of drug and decrease in the encapsulation efficiency. The

sustained drug release was faster and higher in SA-PA-LSA/C-30B/Ag composites compared to other formulations at the temperature 37°C, PT release rate from all of the formulations become faster at 37°C in comparison to room temperature, ensures the SA-PA-LSA/C-30B/Ag composites efficiently deliver the anticancer drug. The drug-loaded composites exhibited "n" values ranging from 0.412 to 0.727 in pH 2 and 0.410 to 0.457 in pH 7.2 indicating the change from Quasi-fickian diffusion type of mechanism to non-fickaian diffusion (Anamalous) type of mechanism and release mechanism of PT drug depends on the dosage form, pH, nature of the drug, fillers, and polymers used.

ACKNOWLEDGMENTS

The authors wish to thank STIC Cochin for providing characterization facility and also we thankful to Amrita School of Engineering, AMC Engineering College, Bengaluru, and Tumkur University, Tumkur, for providing excellent laboratory, library, internet, etc., facilities for successful completion of this project.

AUTHOR CONTRIBUTION

All the author mentioned in this article have equal contributions towards preparation of this article.

CONFLICIT OF INTEREST

Nil

REFERENCES

1. Scognamillo S, Alzari V, Nuvoli D, Mariani A. Thermoresponsive superabsorbent hydrogels prepared by frontal polymerization. J Polym Sci Part A Polym Chem 2010;48:2486-90.
2. Hoffman AS. Hydrogels for biomedical applications. Adv Drug Deliv Rev 2002;54:3-12.
3. Yu L, Zhang Z, Zhang H, Ding J. Biodegradability and biocompatibility of thermoreversible hydrogels formed from mixing a sol and a precipitate of block copolymers in water. Biomacromolecules 2010;11:2169-78.
4. Qiu Y, Park K. Environment-sensitive hydrogels for drug delivery. Adv Drug Deliv Rev 2001;53:321-39.
5. Lammers T, Kiessling F, Hennin WE, Storm G. Drug targeting to tumors: Principles, pitfalls and (pre-) clinical progress. J Controll Release 2012;161:175-87.
6. Gils PS, Ray D, Mohanta GP, Manavalan R, Sahoo PK. Designing of new acrylic-based macroporous superabsorbent polymer hydrogel and its suitability for drug delivery. Int J Pharm Pharm Sci 2009;1:43-54.
7. Lehninger AL, Nelson DL, Cox MM. Principles of Biochemistry. 2nd ed. New York, NY, USA: Worth Publishing; 1993.
8. Liau SY, Read DC, Pugh WJ, Furr JR, Russell AD. Interaction of silver nitrate with readily identifiable groups: Relationship to the antibacterial action of silver ions. Lett Appl Microbiol 1997;25:279-83.
9. McDonnell G, Russell A. Antiseptics and disinfectants: Activity, action, and resistance. Clin Microbiol Rev 2001;12:47-179.
10. Morones JR, Elechiguerra JL, Camacho A, Holt K, Kouri JB, Ramírez JT, *et al.* The bactericidal effect of silver nanoparticles. Nanotechnology 2005;16:2346-53.
11. Wang C, Flynn NT, Langer R. Controlled structure and properties of thermos responsive nanoparticle-hydrogel composites. Adv Mater 2004;16:1074-9.
12. Zhang J, Xu S, Kumacheva E. Photogeneration of fluorescent silver nanoclusters polymer microgels. Adv Mater 2005;17:2336-40.
13. Biffis A, Orlandi N, Corian B. Microgel-stabilized metal nanoclusters: Size control by microgel nanomorphology. Adv Mater 2003;15:1551-5.
14. Paul W, Sharma CP. Chitosan and alginate wound dressings: A short trends biomater. Artif Organs 2004;18:1823.
15. Murata Y, KontaniY, Ohmae H, Shima K. The behavior of alginate gel beads containing chitosan salt prepared with water-soluble vitamins. Eur J Pharm Biopharm 2002;53:249-51.
16. Bajpai SK, Tankhiwale R. Investigation of water uptake behavior and stability of calcium alginate/chitosan bi-polymeric beads: Part-1. React Funct Polym 2006;66:645-58.
17. Satish CS, Satish KP, Shivakumar HG. Hydrogels as controlled drug delivery systems: Synthesis, crosslinking, water and drug transport mechanism. Indian J Pharm Sci 2006;68:133-40.
18. Aminabhavi TM, Kulkarni AR, Soppinath KS. Application of sodium alginate beads crosses linked with glutaraldehyde for controlled release of pesticide. Polym News 1999;24:285-6.
19. Downs EC, Robertson N, Riss TL, Plunkett ML. Calcium alginate beads as a slow-release system for delivering angiogenic molecules *in vivo* and *in vitro*. J Cell Physiol 1992;152:422-9.
20. Babur V, Rao KS, Sairam M. Sodium alginate-poly(hydroxyethyl methacrylate) interpenetrating polymeric network membranes for the pervaporation dehydration of ethanol and tetrahydrofuran. J Appl Polym Sci 2006;99:2671-8.
21. Smidsrod O, Skjak-Braek G. Alginate as immobilization matrix for cells. Trends Biotechnol 1990;8:71.
22. Nanjunda Reddy BH, Lakshmi VV, Vishnu Mahesh KR, Mylarappa M, *et al.*. Nanosyst Physics Chem Math 2016;87:667-74..
23. Miller M, Ojima I. Chemistry and chemical biology of taxane anticancer agents. Chem Rec 2001;3:195-211.
24. Kuhn WC. Therapy for recurrent ovarian cancer. Curr Womens Health Rep 2003;3:33-8.
25. Kongshaug M, Cheng LS, Moan J, Rimington C. Interaction of cremophor EL with human plasma. Int J Biochem 1991;23:473-8.
26. Mankad P, Spatenka J, Slavik Z, Oneil G, Chester A, Yacoub M, *et al*. Acute effects of cyclosporine and Cr EL on endothelial function and vascular smooth muscle in the isolated rat-heart. Cardiovasc Drugs Ther 1992;6:77-83.
27. Jordan MA, Wilson L. Microtubules as a target for anticancer drugs. Nat Rev Cancer 2004;4:253-65.
28. Markman M. Weekly paclitaxel in the management of ovarian cancer. Semin Oncol 2000;27:37-40.
29. Perez EA. Paclitaxel in breast cancer. Oncologist 1998;3:373-89.
30. Singla AK, Garg A, Aggarwal D. Paclitaxel and its formulations. Int J Pharm 2002;235:179-92.
31. Zhang J, Wang Q, Wang A. synthesis and characterization of chitosan-g-poly(acrylic acid)/attapulgite superabsorbent composites. Carbohydr Polym 2007;68:367-74.
32. Abd El-Rehim A, El-Sayed A, Hegazy AM. Selective separation of some heavy metals by poly(vinyl alcohol)-grafted membranes. J Appl Polym Sci 2000;76:125-32.
33. Liu PS, Li L, Zhou NL, Zhang J, Wei SH, Shen J. Waste polystyrene foam-graft-acrylic acid/montmorillonite superabsorbent nanocomposite. J Appl Polym Sci 2007;104:2341-9.
34. CLSI, Wayne. Clinical and Laboratory Standards Institute Methods for Dilution Antimicrobial Susceptibility Tests for Bacteria that Grow Aerobically. Approve Standard M7-A7 CLSI. 7th ed. PA USA; CLSI, Wayne; 2006.
35. Kadam AT, Jadhav RL, Salunke PB, Satwashila S, Sandipand K. Design and evaluation of modified chitosan-based *in situ* gel for ocular drug delivery. Int J Pharm Pharm Sci 2017;9:87-91.
36. Muñoz-Bonilla A, Fernández-García M. Polymeric materials with antimicrobial activity. Prog Polym Sci 2012;37:281-339.
37. Park MV, Neigh AM, Vermeulen JP, de la Fonteyne LJ, Verharen HW, Briedé, and *et al.* The effect of particle size on the cytotoxicity, inflammation, developmental toxicity, and genotoxicity of silver nanoparticles. Biomaterials 2011;32:9810-9817.
38. Shankar S, Rhim JW. Amino acid mediated synthesis of silver nanoparticles and preparation of antimicrobial agar/silver nanoparticles composite films. Carbohydr Polym 2015;130:353-63.
39. Stevanovic M, Savanovic I, Uskokovic V, Skapin SD, Bracko I, Jovanović U, *et al.* A new, simple, green, and one-pot four-component synthesis of bare and poly(α, γ, L-glutamic acid)-capped silver nanoparticles. Colloid Polym Sci 2012;290:221-31.
40. Huang X, Bao X, Liu Y, Wang Z, Hu Q. Catechol-Functional Chitosan/ Silver Nanoparticle Composite as a Highly Effective Antibacterial Agent with Species-Specific Mechanisms. Scientific Reports 7, Article No. 1860.
41. Vimala K, Yallapu MM, Varaprasad K, Reddy NN, Ravindra S, Naidu NS, *et al*. Fabrication of curcumin encapsulated chitosan-PVA silver nanocomposite films for improved antimicrobial activity. J Biomater Nanobiotechnol 2011;2:55-64.
42. Soppimath KS, Kulkarni AR, Aminabhavi TM. Chemically modified polyacrylamide-g-guar gum-based crosslinked anionic microgels as pH-sensitive drug delivery systems: Preparation and characterization. J Control Release 2001;75:331-45.
43. Abdel-Azim AA, Farahat MS, Atta AM, Abdel-Fattah AA. Preparation and properties of two-component hydrogels based on 2-Acrylamido-2-methylpropane sulphonic acid. Polym Adv Technol 1998;9:282.
44. Zhang C, Easteal AJ. Study of free-radical copolymerization of N-isopropylacrylamide with. 2-acrylamido-2-methyl-1-propanesulphonic acid. J Appl Polym Sci 2003;88:2563.

45. Ravindra S, Mulaba-Bafubiandi AF, Rajinikanth V, Varaprasad K, Reddy NN, Raju KM. Development and characterization of curcumin loaded silvernanoparticle hydrogels for antibacterial and drug delivery applications. J Inorg Organomet Polym 2012;22:1254-1262.
46. Yadav M, Rhee KY. Superabsorbent nanocomposite (alginate-g-PAMPS/MMT): Synthesis, characterization and swelling behavior. Carbohydr Polym 2012;90:165-173.
47. Zhang W, Luo S, Fang F, Chen Q, Hu H, Jia X, et al. Total synthesis of absinthin. J Am Chem Soc 2005;127:18-9.
48. Dong ZG, Xu MX, Lei SY, Liu H, Li T, Wang FM, *et al.* Negative refraction with magnetic resonance in a metallic double-ring metamaterial. Appl Phys Lett 2008;92:64101.
49. Sutar PB, Mishra RK, Pal K, Banthia AK. Development of pH-sensitive polyacrylamide grafted pectin hydrogel for controlled drug delivery system. J Mater Sci Mater 2008;19:2247-53.
50. Rehfeldt F, Engler AJ, Eckhardt A, Ahmed F, Discher DE. Cell responses to the mechanochemical microenvironment – implications for regenerative medicine and drug delivery. Adv Drug Deliv Rev 2007;59:1329-39.
51. Reddy BH, Kumar TM, Lakshmi VV. Synthesis and characterization of sodium alginate stabilized nano-ZnO impregnated with bentonite clay. J Bionanosci 2016;11:1-7.
52. Haraguchi K, Takenisa T, Fan S. Effects of clay content on the properties of nanocomposite hydrogels composed of poly(N-isopropylacrylamide) and clay Macromolecules 2002;35:10162.
53. Kabiri K, Zohuriaan-Mehr MJ. Superabsorbent hydrogel composites. Polym Adv Tech 2003;14:438-44.
54. Shankar S, Teng X, Rhim J. Properties and characterization of agar/CuNPs bionanocomposite films prepared with different copper salts and reducing agents. Carbohydr Polym 2014;114:484-92.
55. Elhefian EA, Nasef MM, Yahaya AH. Preparation and characterization of chitosan/agar blended films: Part 2. Thermal, mechanical, and surface properties. E-J Chem 2012;9:510-6.
56. Martucci F, Ruseckai RA. Three-layer sheets based on gelatin and poly (lactic acid), Part 1: Preparation and properties. J Appl Polym Sci 2010;118:3102-10.
57. Swamy TM, Siddaramaiah RB. Sodium alginate and poly (ethylene glycol) blend thermal and morphological behaviors. J Macromol Sci A 2010;47:877-81.
58. Hosseinzadeh H. Controlled release of a poorly water-soluble drug from an amphiphilic and pH-sensitive chitosan-based hydrogel. Int J Pharm Bio Sci 2011;2:1-9.
59. Tang Q, Sun X, Li Q, Wu J, Lin J. Fabrication of a high-strength hydrogel with an interpenetrating network structure. Colloid Surf A 2009;346:91-8.
60. Kulkarni RV, Sa B. Evaluation of pH-sensitivity and drug release characteristics of (polyacrylamide-grafted-xanthan)-carboxy methyl pH sensitive interpenetrating network hydrogel beads. Drug Dev Ind Pharm 2008;34:1406-14.
61. Leonard M, De Boisseson MR, Hubert P, Dalençon F, Dellacherie E. Hydrophobically modified alginate hydrogels as protein carriers with specific controlled release properties. J Control Release 2004;396:395-405.
62. Xu G, Sunada H. Influence of formation changes on drug release kinetics. Chem Pharm Bull 1995;43:483-7.
63. Higuchi T. Mechanism of sustained-action medication. Theoretical analysis of rate of release of solid drugs dispersed in solid matrices. J Pharm Sci 1963;52:1145-9.
64. Korsmeyer RW, Gurny R, Doelker E, Buri P, Peppas NA. Mechanism of solute release from porous hydrophilic polymers. Int J Pharm 1983;15:25-35.
65. Sahoo S, Sahoo R, Nanda R, Tripathy MK, Phani AR. Synthesis and characterization of chitosan polycaprolactone blend for controlled release of ofloxacin drug. Carbohydr Polym 2010;79:106-13.
66. Panigrahy RN, Panda SK, Veerareddy PR. Formulation and *in vitro* evaluation of combined floating-bioadhesive tablets of imatinib mesylate. Int J Pharm Pharm Sci 2017;9:27-33.
67. Rajendra M, Saraswathi B. Formulation and evaluation of fluvoxamine controlled release tablet. Int J Curr Pharm Res 2015;7:47-51.
68. Hago EE, Li X. Interpenetrating polymer network hydrogels based on gelatin and PVA by biocompatible approaches: Synthesis and characterization. Adv Mater Sci Eng 2013;2013:328763.
69. Gandamalla D, Llingabathula H, Yellu NR. Cytotoxicity evaluation of titanium and zinc oxide nanoparticles on the human cell line. Int J Pharm Pharm Sci 2017;9:240-6.
70. Berridge MV, Herst PM, Tan AS. Tetrazolium dyes as tools in cell biology: New insights into their cellular reduction. Biotechnol Annu Rev 2005;11:127-52.